Chemistry & Biodiversity

WILEY-VCH

CHEMISTRY & BIODIVERSITY

RESEARCH ARTICLE OPEN ACCESS

Tandem Mass Spectrometry and Bio-Guided Isolation of Secondary Metabolites With Antiplasmodial Activity From *Dalbergia miscolobium* Bark

Thais Bertolino Vieira Dantas[1] | Igor M. R. Moura[2] | Romário Pereira da Costa[1] | Guilherme Eduardo de Souza[2] | Richele Priscila Severino[1] | Hélder Nagai Consolaro[1] | Luis Felipe de Oliveira[2] | Vinicius Bonatto[2] | Quezia Bezerra Cass[3] | Rafael V. C. Guido[2] | Lorena Ramos Freitas de Sousa[1]

[1]Institute of Chemistry, Federal University of Catalão, Catalão, Brazil | [2]São Carlos Institute of Physics, University of São Paulo, São Carlos, Brazil | [3]Chemistry Department, Federal University of São Carlos, São Carlos, Brazil

Correspondence: Rafael V. C. Guido (rvcguido@usp.br) | Lorena Ramos Freitas de Sousa (lorennarf@ufcat.edu.br)

Received: 27 April 2025 | **Revised:** 13 August 2025 | **Accepted:** 20 August 2025

Funding: This research received financial support from the FAPEG (Goiás State Research Support Foundation) Proc. 202110267000075, FAPESP (The São Paulo Research Foundation, grants #20/12904-5; #24/04805-8; #13/07600-3; #23/15815-1; #23/09209-1, #14/50244-6; #21/03977-1), and the National Council for Scientific and Technological Development (CNPq, Conselho Nacional de Pesquisa e Desenvolvimento), Brazil (302464/2022-0).

Keywords: *Dalbergia miscolobium* | flavonoids | *Plasmodium falciparum* | pyruvate kinase II

ABSTRACT

Strategies have been employed to address antimalarial drug resistance, including the exploration of new therapeutic targets. In this study, the stem bark of *Dalbergia miscolobium* was investigated using in vitro assays against *Plasmodium falciparum* and pyruvate kinase II (PyrKII), an essential enzyme for parasite development. Compounds were dereplicated from ethanolic extract (IC_{50}^{3D7} = 9 μg/mL) using LC-HRMS, revealing active constituents: procyanidin A1 (**2**), biochanin (**5**) and formononetin (**7**). Bio-guided fractionation of the ethyl acetate active fraction (IC_{50}^{3D7} = 8.4 μg/mL) led to the isolation of compounds with antiplasmodial potential, identified by 1D/2D NMR as procyanidin A1 (**2**) (IC_{50}^{3D7} = 42 μM), epicatechin (**9**) (IC_{50}^{3D7} > 50 μM), lupenone (**10**) (IC_{50}^{3D7} = 27 μM) and lupeol (**11**) (IC_{50}^{3D7} = 33 μM). In addition, procyanidin A1 exhibited 90% inhibition of PyrKII catalytic activity at 200 μg/mL. These findings pave the way for the discovery of novel antiplasmodial inhibitors from *D. miscolobium*.

1 | Introduction

Malaria is a parasitic disease caused by *Plasmodium* species, responsible for approximately 263 million cases and 597 000 deaths worldwide in 2023 [1]. The parasites are transmitted through the bites of female *Anopheles* mosquitoes. Effective malaria treatment targets various stages of the *Plasmodium* life cycle, including the interruption of parasite replication in red blood cells, the elimination of latent hypnozoites in *Plasmodium vivax* and *Plasmodium ovale*, and the prevention of gametocyte development [2].

The emergence of drug-resistant malaria strains underscores the urgent need to explore alternative metabolic pathways to disrupt parasite development [3–5]. One promising target is pyruvate kinase II (PyrKII), an enzyme located in the apicoplast, which plays a critical role in the synthesis of essential biomolecules involved in the parasite's metabolism, such as lipids

Thais Bertolino Vieira Dantas and Igor M. R. Moura contributed equally to this work.

and nucleotide triphosphate (NTP) derivatives [6–10]. Genetic deletion studies have demonstrated that PyrKII is essential for maintaining organelle integrity during the blood stage of parasite development. Its absence leads to organelle rupture and subsequent parasite death, highlighting its potential as target for novel antimalarial therapies [11]. In the search for new PyrKII inhibitors as lead candidates for malaria drug discovery, the investigation of natural products (NPs) is particularly relevant, especially considering the significant number of existing antimalarial drugs derived from natural sources [6, 12–15]. Species from *Dalbergia* genus (Fabaceae) have demonstrated antiplasmodial potential, with isoflavones and neoflavones identified as key secondary metabolites [16]. *Dalbergia miscolobium* Benth, commonly known as "jacarandá-do-cerrado," is an endemic species widely distributed in the Cerrado biome. However, knowledge about its chemical composition and biological potential remains limited [17, 18]. Previous studies have identified triterpenes, diterpenes, and the isoflavonoid prunetin in the leaves. Isoflavonoids, including isoflavones and isoflavans, have also been isolated from the branches, alongside known terpenes and steroids [18]. Isoflavonoids are considered chemotaxonomic markers of the Fabaceae family (subfamily *Papilionoideae*) and have been reported in 31 species of the *Dalbergia* genus [19].

Previoulsy, ethanolic extracts from *Dalbergia* species have demonstrated antiplasmodial activity [16]. In this study, the inhibitory activity of the crude ethanolic extract (EtOH) obtained from the stem bark of *D. miscolobium* was evaluated in vitro against *Plasmodium falciparum*, revealing its inhibitory potential and antiplasmodial activity. The active extract was dereplicated using liquid chromatography coupled with high-resolution mass spectrometry (LC-HRMS). Furthermore, to identify the active compounds responsible for the observed activity, a bioactivity-guided fractionation was performed using the chloroquine-sensitive *P. falciparum* 3D7 strain.

2 | Results and Discussion

2.1 | Chemical Prospection of Active Extract by LC-HRMS

Several *Dalbergia* species have demonstrated antiplasmodial activity, including *D. louvelii* [16]. However, *D. miscolobium* has not previously been investigated against *Plasmodium* spp. In this study, a crude ethanolic extract from the stem bark of *D. miscolobium* (*Dm*Eb) was prepared and tested in vitro against the *P. falciparum* 3D7 strain (chloroquine-sensitive). The extract (*Dm*Eb) exhibited 93 ± 1% inhibition at a concentration of 50 µg/mL and an IC_{50}^{3D7} value of 9.0 ± 0.1 µg/mL, which is considered highly promising based on the parameters established by Singh et al. [20, 21] The cytotoxicity of DmEb extract was evaluated against HepG2 cells, showing moderate inhibition (CC_{50}^{HepG2} = 53 ± 13 µg/mL), with a selectivity index (SI) of 6. To determine the chemical profile of the active extract, tandem mass spectrometry (LC-HRMS) was employed for compound dereplication. MS/MS data acquired in negative ionization mode $[M-H]^-$ were analyzed and compared with free compound screening libraries using the CompoundCrawler software (https://www.ebi.ac.uk/chebi/, https://www.chemspider.com/, https://www.genome.jp/kegg/, https://pubchem.ncbi.nlm.nih.gov/) as well as with data available in the literature. Eight compounds were annotated from the extract, including flavonoids, terpenoids, and phenolic derivatives: proanthocyanidin (**1**) [22], procyanidin (**2**) [22, 23], methoxy-trihydroxyflavone (**3**) [24, 25], dimethoxy-hydroxyacetophenone (**4**) [26], dihydroxy-methoxyisoflavone (biochanin) (**5**) [24, 27, 28], dihydroxy-dimethoxyisoflavanone (**6**) [24], hydroxy-methoxyisoflavone (formononetin) (**7**) [24, 29], and isomer of phytuberin (**8**) [30] (Table 1; Figures S15S–S22).

Compound **1** was assigned based on its deprotonated molecular ion at *m/z* 863.1829 ($C_{45}H_{36}O_{18}$) and the following product ions: *m/z* 711.1378 (resulting from retro-Diels-Alder [RDA] cleavage), 573.1039, 451.1016, 411.0717, 289.0717 [22]. Proanthocyanidins are flavan-3-ol polymers commonly found in the *Dalbergia* genus, including species such as *Dalbergia monetaria* and *Dalbergia boehmii* [31–35].

Compound **2** was annotated with a characteristic ion at *m/z* 575.1195 ($C_{30}H_{24}O_{12}$), and exhibited fragment ions at *m/z* 449.0879, 423.0707, 289.0710, and 109.0306. The ion at *m/z* 449.0879 is associated with heterocyclic ring fission, while the ion at *m/z* 289.0710 corresponds to cleavage of the epi/catechin unit. The ion at *m/z* 423.0707, resulting from an RDA rearrangement, supported the annotation of this compound as procyanidin [22, 23]. Compound **2** was isolated from the ethyl acetate fraction (*Dm*A) and was also fully characterized in this study using 1D and 2D NMR spectroscopy. Procyanidin is known for its antiplasmodial activity [31], and its presence in the crude extract supports the observed biological potential.

Compound **3** was annotated based on its deprotonated molecular ion at *m/z* 299.0561 ($C_{16}H_{12}O_6$) and the fragment ions: *m/z* 284.0308 (−15.0253 Da, loss of CH_3), 283.0232, 256.0337, 255.0294, 151.0055, and 147.0097, in comparison with literature data [25, 28]. The fragmentation behavior of compound **3** suggests it is a methoxylated flavone derivative of luteolin, likely chrysoeriol, whose aglycone and the glycoside forms have been reported in *Dalbergia stipulacea* [36]. Compounds from the isoflavone and flavone classes are commonly found in the *Dalbergia* genus, and isoflavones have been specifically identified in *D. miscolobium* [37]. The presence of isoflavones reinforces the phytochemical consistency and chemotaxonomic classification of the *Dalbergia* genus, as these secondary metabolites are known chemotaxonomic markers for the Fabaceae family [19].

Compound **4** was annotated as dimethoxy-hydroxyacetophenone (acetosyringone) [30] based on its deprotonated molecular ion at *m/z* 195.0664 ($C_{10}H_{12}O_4$), and characteristic fragment ions at *m/z* 180.0414, 167.0347, 152.0105, 136.0161, 135.0091, and 121.0296. In the MS^2 spectrum, the loss of the acetyl group (−43.0558 Da) is evidenced by the signal at *m/z* 152.0105. From this ion, a further fragment at *m/z* 135.0091 was generated by the loss of a hydroxyl group [M−17]. The product ion at *m/z* 180.0414 corresponds to the loss of a methyl group [M−15]. Phenolic derivatives have previously been identified in *D. odorifera* [38]. Although acetosyringone has demonstrated antibacterial activity, particularly against *Pseudomonas* species, there are no reports of its antiprotozoal activity [39].

Compounds **5**, **6**, and **7** were annotated based on their deprotonated molecular ions at *m/z* 283.0612 ($C_{16}H_{12}O_5$), *m/z* 315.0874

TABLE 1 | Compounds identified in the extract *Dm*Eb by LC-HRMS.

Cpd	RT (min)	Formula	Observed m/z $[M-H]^-$	Calculated m/z $[M-H]^-$	Error (ppm)	Product ion in MS/MS spectra	Annotation
1	5.3	$C_{45}H_{36}O_{18}$	863.1829	863.1831	0.8	711.1378; 573.1039; 451.1016; 411.0717; 289.0717	Proanthocyanidin
2	6.7	$C_{30}H_{24}O_{12}$	575.1195	575.1198	−0.5	449.0879; 423.0707; 289.0710; 109.0306	Procyanidin
3	7.2	$C_{16}H_{12}O_6$	299.0561	299.0555	2.0	284.0308; 283.0232; 256.0337; 255.0294; 151.0055; 147.0097	Methoxy-trihydroxyflavone
4	8.0	$C_{10}H_{12}O_4$	195.0664	195.0666	−1.7	180.0414; 167.0347; 152.0105; 136.0161; 135.0091; 121.0296	Dimethoxy-hydroxyacetophenone
5	9.2	$C_{16}H_{12}O_5$	283.0612	283.0612	0.1	268.0372; 240.0415; 239.0345; 211.0400; 151.0022; 131.0140	Dihydroxy-methoxyisoflavone
6	9.7	$C_{17}H_{16}O_6$	315.0874	315.0870	1.2	300.0576; 285.0397; 135.0088; 165.0180; 149.0241	Dihydroxy-dimethoxyisoflavanone
7	11.8	$C_{16}H_{12}O_4$	267.0663	267.0664	−0.6	252.0419; 224.0457; 223.0401; 195.0453; 135.0089	Hydroxy-methoxyisoflavone
8	13.8	$C_{17}H_{26}O_4$	293.1758	293.1754	1.4	236.1050; 221.1545; 192.1155	Phytuberin

Note: The MS^2 spectra data described in this table were analyzed by using the programs CompoundCrawler and Data Analysis 4.
Abbreviations: Cpd, compound; *Dm*Eb, crude ethanolic extract from the stem bark of *Dalbergia miscolobium*; RT, retention time.

($C_{17}H_{16}O_6$), and m/z 267.0663 ($C_{16}H_{12}O_4$), respectively, along with characteristic fragment ions consistent with isoflavonoids structures [24, 27–29]. For compound **5**, the fragment ions were observed at m/z 268.0372 (−15.0240 Da, loss of CH_3), and 240.0415 (−27.9957 Da, loss of CO). A subsequent loss of a hydrogen radical yielded the ion at m/z 239.0345. From this fragment, the product ion at m/z 211.0400 was generated (−27.9945 Da, further loss of CO), which is consistent with fragmentation at ring C, resulting in two hydroxyl groups remaining on ring A. The distinction between biochanin and its isomer, glycitein, was observed through differences in their fragment ion patterns, particularly the lack of the product ion at m/z 147, which is typically associated with the presence of a methoxy group at C_6 of ring A in glycitein [24]. Although RDA-derived fragments were detected at lower abundance (m/z 151.0022 and m/z 131.0140), they still supported the presence of two hydroxyl groups on ring A and a methoxy group on ring B, respectively [24, 28].

TABLE 2 | Percentage of inhibition (%), antiplasmodial activity (IC_{50}^{3D7}), cytotoxicity (CC_{50}^{HepG2}), and selectivity index (IS) of fractions obtained from ethanolic extract *Dm*Eb.

Extract	Inhibition (%), 50 μg/mL	IC_{50}^{3D7} (μg/mL), mean ± SD	CC_{50}^{HepG2} (μg/mL), mean ± SD	SI
*Dm*H	95 ± 2	1.7 ± 0.6	30 ± 3	17
*Dm*A	93 ± 1	8.4 ± 0.7	59 ± 11	7
*Dm*Ha	61 ± 7	46 ± 3	54 ± 16	1
ART	99 ± 1	15 ± 5 nM	nd	nd

Abbreviations: ART, artesunate (positive control); *Dm*A, ethyl acetate; *Dm*H, hexane; *Dm*Ha, hydroalcoholic fractions; nd, not determined.

For compound **6**, the product ions were observed at *m/z* 300.0576 (15.0298 Da, loss of CH_3), 285.0397, 257.0459, and 135.0088. The loss of methyl group is a common fragmentation pathway in methoxylated flavonoids. In addition, cleavage of ring C by RDA rearrangement generated product ions at *m/z* 165.0180 and *m/z* 149.0241, which allowed the prediction of a substitution pattern consisting of one hydroxyl and one methoxyl group on each of rings A and B, characteristic of the cajanol structure (Figure S14) [24, 28]. The MS^2 spectrum of compound **7** showed fragment ions at *m/z* 252.0419, 224.0457 (−27.9962 Da, loss of CO), 223.0401, and 135.0089. The product ion at *m/z* 135.0089 is consistent with RDA cleavage of ring C, suggesting the presence of a single hydroxyl group on ring A [24, 29]. Biochanin (**5**) and formononetin (**7**) have previously been identified in *D. odorifera* [38, 40]. However, to date, there have been no reports of these secondary metabolites in *D. miscolobium*.

Biochanin (**5**) and formononetin (**7**) have demonstrated antiplasmodial activity against the chloroquine-sensitive *P. falciparum* poW strain. Compound **5** exhibited an IC_{50}^{poW} value of 46.8 μg/mL, while compound **7** showed an IC_{50}^{poW} value greater than 50 μg/mL [41]. In addition, cajanol (**6**) has also been evaluated for its antiplasmodial potential but exhibited poor in vitro inhibitory activity (IC_{50} > 100 μM) [42].

Terpenoid **8** showed a deprotonated molecular ion at *m/z* 293.1758 ($C_{17}H_{26}O_4$). The MS^2 spectrum revealed characteristic fragment ions consistent with phytuberin [30], including those at *m/z* 236.1050, 221.1545, and 192.1155. The loss of an acetate unit (−57.0708 Da) was evidenced by the peak at *m/z* 236.1050. This fragment subsequently generated a product ion at *m/z* 221.1545, corresponding to the loss of a methyl (−14.9505 Da). The signal at *m/z* 192.1155 resulted from the loss of an isopropyl acetate group (−101.0603 Da). Phytuberin (**8**) has previously been identified in *Cyphomandra betacea*, and structurally related sesquiterpenoids are known to occur in *D. odorifera* [26, 38].

2.2 | Bio-Guided Fractionation of Active Fractions

The ethanolic extract (*Dm*Eb, IC_{50}^{3D7} of 9.0 ± 0.1 μg/mL) was subjected to liquid–liquid partitioning, yielding hexane (*Dm*H), ethyl acetate (*Dm*A) and hydroalcoholic fractions (*Dm*Ha), which were evaluated for their antiplasmodial activity and cytotoxicity (Table 2). Among these, *Dm*H and *Dm*A demonstrated promising activity against the *P. falciparum* 3D7 strain, with 95 and 93% inhibition at 50 μg/mL, respectively. The half-maximal inhibitory concentrations (IC_{50}^{3D7}) were determined to be 1.7 and 8.4 μg/mL, respectively (Table 2). The cytotoxic effects of *Dm*H and *Dm*A were assessed against HepG2 cells, showing moderate inhibition ($CC_{50}s^{HepG2}$ of 30 and 59 μg/mL, respectively), with SIs of 17 and 7, respectively (Table 2).

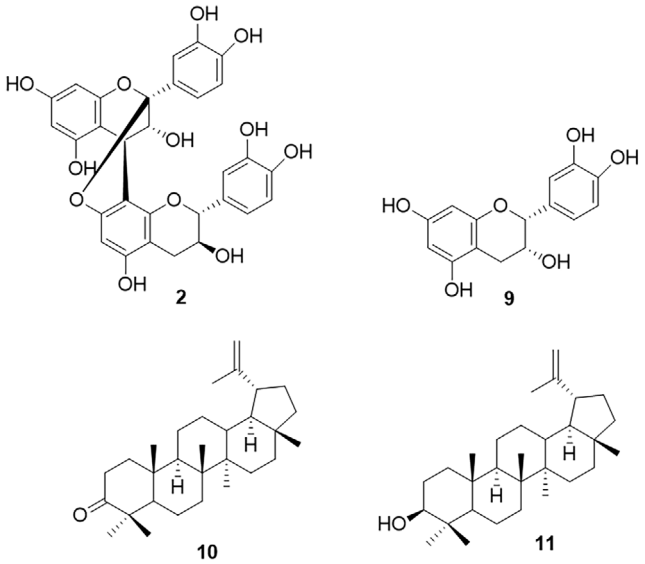

FIGURE 1 | Active compounds isolated through bioguided-fractionation of the active EtOAc fraction of *Dalbergia miscolobium*.

Phytochemical analysis of the EtOAc fraction (*Dm*A) led to active subfractions (Figures S1 and S2; Tables S1–S3), some of which enhanced the antiplasmodial potential. These subfractions afforded active flavonoids, including procyanidin (**2**) and epicatechin (**9**), as well as terpenoids such as lupenone (**10**) and lupeol (**11**) (Figure 1).

The ESI-TOF-MS data showed a protonated ion $[M+H]^+$ at *m/z* 577 ($C_{30}H_{24}O_{12}$) for compound **2**. The ^1H NMR spectrum revealed two ABX systems in the aromatic region (δ_H 6.8–7.1), a singlet at δ_H 6.09 (s, H-6′), and meta-coupled doublets at 6.02 and 6.08 ppm (each d, *J* = 3.0 Hz, H-6 and H-8) characteristic of procyanidin [29]. The first flavonoid moiety exhibited a broad singlet at δ_H 4.26 (s, H-4) and the proton at δ_H 4.07 (d, *J* = 5.4 Hz, H-3), suggesting an epicatechin unit. The coupling constants of the diastereotopic protons at δ_H 2.75 and δ_H 2.94 (dd, *J* = 16.8 and 7.0 Hz for H-4′α and *J* = 17.0, 3.6 Hz for H-4′β) together with the multiplet at δ_H 4.10 (m, H-3′) and a doublet at δ_H 4.40 (d, *J* = 4.8 Hz, H-2′), indicate a catechin-type isomer.

^{13}C NMR data obtained from HSQC and HMBC projections (Figures S3–S7), including long-range heteronuclear correlations between the proton at δ_H 4.26 (s, H-4) and the carbons at δ_c 106.3 (C-8′) and 150.8 (C-8′a), confirmed the structure as procyanidin A1. Notably, this is the first report of procyanidin A1 in the species *D. miscolobium*. Compound **2** exhibited moderate antiplasmodial activity, with an $IC_{50}{}^{3D7}$ value of 24 μg/mL (42 μM), and showed 90% inhibition of PyrKII at 200 μg/mL (347 μM).

The ^{1}H NMR spectrum of compound **9** exhibited an ABX system with signals at δ 6,75 (d, J = 8 Hz, H-5′), δ 6,79 (dd, J = 2 Hz and 8 Hz, H-6′), and δ 6,97 (d, J = 1.8 Hz, H-2′). For ring A, a meta-coupling pattern of aromatic protons was observed at δ 5.94 (d, J = 2.16 Hz, H-6) and δ 5.92 (d, J = 2.16 Hz, H-8). The low coupling constants of the C-ring protons at δ 2.71 (dd, J = 2.76 Hz, 16.9 Hz, H-4α), δ 2.84 (dd, J = 4.76 Hz, 16.9 Hz, H-4β) and δ 4.16 (m, J = 1.4 Hz, H-3) suggested an epicatechin skeleton [43]. The antiplasmodial activity of epicatechin has been previously reported, with an IC_{50} > 50 μM [44]. Structurally related compounds, such as epigallocatechin gallate and epicatechin gallate, have also been evaluated, exhibiting $IC_{50}{}^{3D7}$ values of 37 and 11 μM, respectively [45].

Compounds **10** and **11** were isolated as white powders and identified based on ^{1}H and ^{13}C NMR data obtained from HSQC and HMBC projections. The chemical shifts of both protons and carbons (Figures S8–S13; Tables S4 and S5) were compared with literature data [46–48]. The ^{1}H NMR spectrum of compound **10** showed seven methyl singlets between δ 0.98 and 1.72, and vinylic protons at δ 4.55 (m, H-29b) and 4.68 (d, J = 2,4 Hz, H-29a). Heteronuclear correlations between the protons at δ 0.98 (H-24) and 1.02 (H-23) with the carbonyl group at δ 216.8 (C-3), and with the olefinic carbons at δ 151.6 (C-20) and 109.6 (C-29), supported the identification of a lupenone skeleton.

The ^{1}H NMR spectrum of compound **11** revealed seven methyl singlets between δ 0.74 and 1.64, and a doublet of doublets at δ 3.14 (dd, J = 5.16, 11.12 Hz, H-3). Olefinic protons appeared at δ 4.49 and 4.61, while the corresponding carbons were observed at δ 150.0 and 108.4; in addition, a signal at δ 78.4 (C-3) was consistent with the presence of a hydroxylated carbon. These data supported the assignment of a lupeol structure. Compound **10** was previously identified in the *n*-hexane extract from the bark of *D. miscolobium*, while compound **11** was isolated from the leaves of the same species [17, 18].

Lupenone (**10**) and lupeol (**11**) exhibited promising activity against the *P. falciparum* 3D7 strain, with $IC_{50}{}^{3D7}$ values of 27 and 33 μM, respectively. Furthermore, both compounds showed low cytotoxicity toward hepatocarcinoma cells ($CC_{50s}{}^{HepG2}$ > 100 and > 50 μg/mL, respectively). In line with these results, the antiplasmodial activity of lupenone has previously been reported against the W2, D6, and K1 strains of *P. falciparum* [49], while lupeol has demonstrated inhibitory activity in the schizont maturation assay [21].

The *Dm*H fraction was further investigated by GC–MS, which enabled the dereplication of three esters: compounds **12**, **13**, and **14**. Compound **12** was assigned as ethyl hexadecanoate, exhibiting a molecular ion peak at m/z 284 and molecular formula $C_{18}H_{36}O_2$, with characteristic fragment ions at m/z 55, 73, 88, 101, 157, and 241. The peak at m/z 88 is attributed to a McLafferty rearrangement (−196 Da), followed by the loss of CH_3 group, generating a product ion at m/z 73. Compounds **13** and **14** were assigned as ethyl linoleate (**13**) and ethyl elaidate (**14**), respectively, with molecular ion peaks at m/z 308 and m/z 310, and fragment ions characteristic of esters functionalities [17, 50–53].

Structurally related carboxylic acid derivatives have previously been reported in *D. miscolobium* [17]. These compounds also exhibit reported biological activities, including antibacterial and antioxidant properties [53, 54]. Furthermore, antiplasmodial activity has been shown to be more pronounced in carboxylic acid derivatives with a higher degree of unsaturation [55].

Compounds isolated from *D. miscolobium* extract showed inhibitory activity in the micromolar range, whereas standard antimalarials such as chloroquine and artesunate act in the low nanomolar range. Nonetheless, the structural diversity and novelty of these NPs represent valuable scaffolds that could be optimized to enhance potency. Targeting key metabolic pathways in the parasite may provide new opportunities for antimalarial drug development [56, 57]. In this context, PyrKII is an understudied enzyme within the *P. falciparum* druggable genome [58], and no inhibitors have been reported to date. Therefore, these findings may serve as a starting point for the discovery of novel PyrKII inhibitors as potential lead candidates for antimalarial therapy.

2.3 | Molecular Modeling of Procyanidin A1 Binding to PyrKII

To gain structural insights into the binding mode and affinity of procyanidin A1 (**2**) toward PyrKII, a molecular docking study was performed. Due to the ligand's molecular size and polarity, KVFinder [59, 60] was used to identify potential binding pockets. The analysis revealed that the PyrKII active site was the largest and most accessible cavity. Notably, the active site contains a Mg^{2+} ion (cofactor), which is known to coordinate electronegative groups, making it particularly relevant for interactions with the phenolic substituents present in procyanidin A1. Docking results (Figure 2) showed a binding pose where one hydroxyl group of procyanidin A1 coordinates with the Mg^{2+} ion. This hydroxyl group also forms a hydrogen bond with the side chain of Asp376, which may enhance the electron density on the coordinating oxygen and promote coordination with the metal ion. Additional hydrogen bonds were observed between the ligand and the side chains of Arg416 and His35, as well as between another phenolic group and the backbone carbonyl of Ile8. These findings suggest that procyanidin A1 is capable of binding to the active site and may act as a competitive inhibitor with ATP. However, further experimental validation is required to confirm this mechanism of inhibition.

3 | Conclusions

This study demonstrated the antiplasmodial potential of the crude extract and its hexane and ethyl acetate fractions from the stem bark of *D. miscolobium*. Through an integrated approach

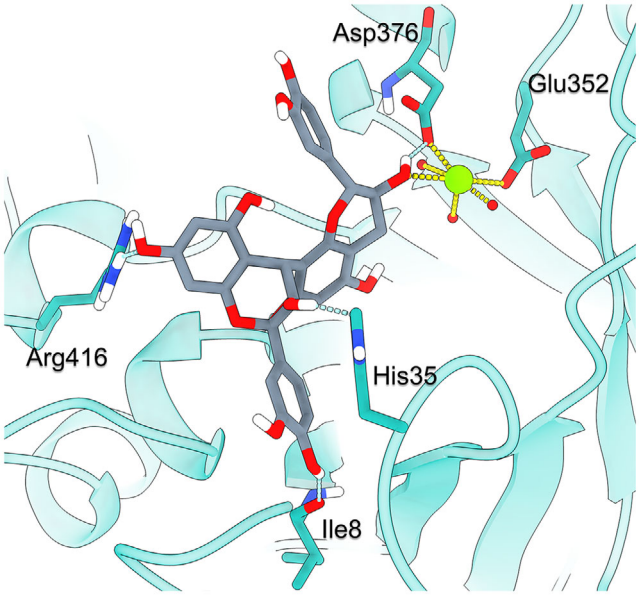

FIGURE 2 | Predicted binding pose of procyanidin A1 in the active site of *Pf*PyrKII. The Mg^{2+} cofactor is depicted as a green sphere. Coordination bonds between the ligand, Asp376, Glu352, and three structural water molecules are shown as yellow dashed lines. Hydrogen bonds are indicated by cyan dashed lines. The ligand is displayed in stick representation, and key interacting residues are labeled.

combining in vitro assays, LC-HRMS, and bio-guided fractionation, several active compounds were identified. LC-HRMS analysis of the crude extract revealed isoflavones such as biochanin and formononetin, known chemotaxonomic markers of the Fabaceae family, with antiplasmodial activity. From the EtOAc fraction, structurally diverse compounds with antiplasmodial potential were isolated and characterized by NMR spectroscopy, including procyanidin A1, lupenone, and lupeol. Notably, procyanidin A1 exhibited moderate inhibition of the PyrKII enzyme, suggesting this kinase as a possible molecular target contributing to its antiplasmodial activity. Altogether, these findings highlight *D. miscolobium* as a promising natural source of antiplasmodial compounds, supporting the bioprospecting of this genus and strengthening the link between NPs and antimalarial drug discovery.

4 | Experimental Section

4.1 | General Experimental Materials, Equipment, and Chemicals

Isolation procedures were carried out using Silica gel 60 (70-230 mesh, Macherey-nagel GmbH & Co. KG, Düren, Germany), Sephadex LH-20 (Sigma-Aldrich, St. Louis, MO, USA) and cellulose (200–400 mesh; Sigma-Aldrich). Thin-layer chromatography (TLC) was employed to monitor isolation process, using silica gel 60 F_{254} precoated aluminum plates (Fluka, Sigma-Aldrich). TLC spots were visualized under $UV_{254/365}$ light (Spectroline ENF-260C) and by spraying with a sulfuric acid–vanillin solution, followed by heating. All solvents used in the extraction and isolation procedures were purchased from Dinâmica (Indaiatuba, SP, Brazil) and Vetec (Duque de Caxias, RJ, Brazil). ^{1}H and ^{13}C NMR spectra (1D and 2D) were recorded in MeOH-d_4, $CDCl_3$, acetone-d_6 and DMSO-d_6 (Cambridge Isotope Laboratories Tewksbury, MA, USA or Deutero GmbH, Kastellaun, Germany) on a Bruker 400 MHz spectrometer Ascend model (Bruker Biospin GmbH, Rheinstetten, Germany) and on a Bruker 600 MHz spectrometer (14.1 T) using TMS as the internal reference.

LC-HRMS analyses were performed using a 1290 Infinity II UHPLC system (Agilent, Barueri, SP, Brazil) coupled to a high-resolution quadrupole time-of-flight mass spectrometer (QTOF Impact HD) with an electrospray ionization (ESI) source (Bruker Daltonics, Bremen, Germany) (FAPESP 2014/50244-6). Compound purification was performed using a Shimadzu HPLC system equipped with an LC-20AR pump, an SIL-10AF autosampler, and an SPD-M20A photodiode array detector.

GC–MS analyses were carried out using an Agilent 5975 MSD systems (Agilent Technologies, Santa Clara, CA, USA), operating in electron impact mode (IE, ionization energy 70 eV, source temperature 230°C). Chromatograms and mass spectra were processed using Enhanced ChemStation software (MSD ChemStation E.02.02.1431, Agilent Technologies).

4.2 | Plant Material

The stem bark of *D. miscolobium* was collected on May 26, 2021, in Catalão, Goiás, Brazil (coordinates: 18°09′48.5″ S; 47°55′04.8″ W). The species was identified by H. N. Consolaro, and a voucher specimen (Voucher # 244503) was deposited at the Herbarium of the University of Brasilia (UB), UnB. Access to the genetic patrimony was registered in the SISGEN database (https://sisgen.gov.br/) under registration code A96F19E.

4.3 | Extraction and Isolation

Air-dried and powdered stem bark of *D. miscolobium* (1.2 kg) was subjected to maceration with ethanol for 9 days, with solvent replacement every 3 days. The ethanolic extract was concentrated under reduced pressure using a rotatory evaporator at 40°C to yield a crude extract after complete solvent removal. The dried extract was subjected to antiplasmodial assay and LC-HRMS analysis.

The active ethanolic extract ($IC_{50}{}^{3D7}$ = 9.0 ± 0.1 µg/mL; 70 g) was suspended in a mixture of ethanol and water (EtOH/H_2O, 1:3 v/v) and sequentially partitioned by liquid–liquid extraction with hexane and ethyl acetate (EtOAc). This procedure yielded three fractions: hexane (0.54 g), ethyl acetate (57 g), and hydroalcoholic (EtOH/H_2O) (7.86 g).

The EtOAc fraction from stem bark showed significant antiplasmodial activity ($IC_{50}{}^{3D7}$ = 8.4 ± 0.7 µg/mL). Due to the substantial yield and polarity suitable for biological assays, this fraction was selected for bioactivity-guided fractionation. Chromatography procedures were monitored by TLC and in vitro assays against *P. falciparum* 3D7 strain. EtOAc fraction (4.76 g) was subjected to Sephadex LH-20 column chromatography (26.5 × 5.7 cm, MeOH, isocratic), affording 21 subfractions (A1–A21). Among them, subfractions A16 and A20 were identified as flavonoids **9**

(43.8 mg, IC_{50} > 50 μM) and **2** (353 mg), respectively. Compound **2** was further purified by semi-preparative HPLC using a Gemini C18 column (5 μm, 110 Å, 250 × 10 mm; Phenomenex, CA, USA) and a gradient elution of H_2O (A) and acetonitrile (ACN, B) with a flow rate of 2.0 mL/min. The gradient increased from 20% to 100% of B over the run, followed by 1 min at 100% B for column cleaning, and a 10 s re-equilibration to initial conditions (20% B). This process afforded 1.4 mg of compound **2** (IC_{50}^{3D7} = 24.0 μg/mL).

Active subfraction A9 (274.2 mg, IC_{50}^{3D7} = 4.2 ± 0.2 μg/mL) was further chromatographed on silica gel (22 × 2.5 cm; hexane/ethyl acetate, 9:1), yielding 26 subfractions. Subfraction 11 was identified as the triterpene **10** (3.6 mg, IC_{50}^{3D7} = 26.6 μM).

In addition, a larger portion of the EtOAc fraction (10.54 g) was subjected to cellulose column chromatography (18.50 × 8.7 cm; hexane/EtOAc, 1:1), yielding six subfractions (B1–B6). The active subfraction B2 (IC_{50}^{3D7} = 3.2 ± 0.04 μg/mL) was fractionated on silica gel column (17 × 3.7 cm; hexane/EtOAc, 9:1), affording 34 subfractions. Subfraction eight was identified as the triterpene **11** (9.5 mg, IC_{50}^{3D7} = 33.3 μM). The isolated compounds were characterized by ^1H and ^{13}C NMR, DEPT-135, HSQC, and HMBC experiments, and their spectral data were compared with previously reported literature values [29, 43, 46–48].

4.4 | Chemical Dereplication by LC-HRMS

The analysis was performed using a Cortecs C18+ analytical column (2.7 μm particle size; 100 × 2.1 mm; Waters, Milford, MA, USA). The mobile phase consisted of 0.1% formic acid in water (solvent A) and 0.1% formic acid in acetonitrile (solvent B). The elution was carried out using a linear gradient from 5% to 100% B over 26 min. The flow rate was set to 0.4 mL/min, with a temperature of 40°C and an injection volume of 5 μL.

Ionization experiments were conducted in negative ion mode $[M-H]^-$, with the following ESI source parameters: capillary voltage, 4500 V; quadrupole energy, 5 eV; collision cell energy, 5 eV; transfer time, 50 and 90 μs; pre-pulse time: 6 μs; nebulization pressure, 4 bar; drying gas flow, 8 L/min; and source temperature, 180°C. Full-scan MS data were acquired over an m/z range of 50–1300. Data dependent MS/MS acquisition was performed in automatic mode using a 3-s time cycle, with collision energies of 20, 25, 30, 35, and 40 eV applied across the full m/z range. For internal calibration, sodium formate (1 mM) was used. Compound identification from the crude extract was performed using Bruker Smart Formula 3D, CompoundCrawler and DataAnalysis 4.0 software (Bruker Daltonics, Bremen, Germany).

4.5 | GC–MS Analysis

Injections were performed in *split* mode using the following oven temperature conditions: initial temperature of 60°C (held for 2 min), followed by a ramp of 4°C/min to 70°C, then 25°C/min to 200°C, and 4°C/min to 300°C, with a final isothermal hold for 2 min. Helium was used at a flow rate of 1.0 mL/min. Separation of the sample's chemical constituents was carried out using an HP-5MS capillary column (30 m × 250 μm i.d., 0.25 μm film thickness; Agilent).

Data acquisition was performed in scan mode over an m/z range of 50–600. Compound identification from the hexane fraction was based on comparison of the experimental mass spectra with entries in the NIST Mass Spectral Library 2.0. Retention indices were also determined using hydrocarbon standards (Sigma-Aldrich) injected under identical analytical conditions.

4.6 | In Vitro Assay in *P. falciparum*

The *P. falciparum* 3D7 strain was maintained in culture at 37°C in a humidified incubator using RPMI-1640 medium supplemented with 25 mM $NaHCO_3$, 25 mM HEPES (pH 7.4), 11 mM glucose, 3.67 mM hypoxanthine, 50 μg/mL gentamicin, and 0.5% (w/v) Albumax II. Culture medium was replaced daily, and parasitemia was maintained below 10% at a hematocrit of 2.5% using O^+ human erythrocytes. Parasites were synchronized using the sorbitol method [61] and cultures were adjusted to 0.5% parasitemia and 2% hematocrit for assays.

Antiplasmodial activity was assessed by adding 180 μL of the parasites culture to each well of a 96-well plate, followed by 20 μL of 10× concentrated compound solutions. Negative controls included non-parasitized erythrocytes and untreated infected cultures were set up in parallel. The final DMSO concentration in all wells was kept below 0.05%. Plates were incubated for 72 h at 37°C in a humidified atmosphere containing 5% CO_2. After incubation, the culture medium was removed, and cells were resuspended in 100 μL of PBS buffer. Lysis was achieved by adding 100 μL of lysis buffer containing 0.002% (v/v) SYBR Green I. Plates were incubated at room temperature for 30 min, and fluorescence (proportional to parasite density) was measured using a SpectraMAX Gemini EM plate reader (excitation at 485 nm and emission at 535 nm). IC_{50}^{3D7} values were determined by nonlinear regression of concentration-response curves using Origin 2016 software (OriginLab Corporation).

4.7 | In Vitro Cytotoxicity Evaluation

Hepatoma cells (HepG2) were cultured in RPMI medium supplemented with 10% (v/v) fetal bovine serum and 0.2% (v/v) penicillin/streptomycin at 37°C and 5% CO_2. Cells were transferred into 96-well plates at a density of 10 000 cells/well and incubated at 37°C for 24 h to allow adhesion. Subsequently, the plates were incubated in different concentrations of the tested materials (ranging from 400 to 1.6 μg/mL) for 72 h at 37°C and 5% CO_2. Cytotoxicity was evaluated using a colorimetric assay based on cellular metabolic activity, employing 3-(4,5-dimethylthiazol-2-yl)-2,5-diphenyltetrazolium bromide (MTT). A volume of 20 μL of MTT solution (5 mg/mL) was added to each well, followed by incubation for 3–5 h at 37°C.

After incubation, the supernatant was removed, and the formazan crystals formed were solubilized in 100 μL of DMSO. Absorbance, which correlates with the number of viable cells, was measured using a SpectraMAX Plus 384 plate reader (λ = 570 nm) [62]. The CC_{50}^{HepG2} value was determined by nonlinear regression analysis of the dose-response curve using GraphPad Prism 8 software. The SI was calculated as the ratio between cytotoxicity and antiplasmodial activity ($SI = CC_{50}^{HepG2}/IC_{50}^{3D7}$).

4.8 | Expression and Purification of PyrKII

The gene encoding *P. falciparum* PyrKII (*Pf*PyrKII), cloned into the pMAL-cHT expression vector, was kindly donated by Professor Dr. Sean Prigge (Johns Hopkins University). Briefly, PyrKII expression was carried out in *Escherichia coli* BL21 Rosetta (DE3) strain in LB medium with the addition of pRIL supplementary plasmid. Selected colonies containing both plasmids, pMAL-cHT-PKII (ampicillin resistant) and pRIL (chloramphenicol resistant), were grown in LB medium at 37°C with shaking at 220 rpm. At an OD_{600} of 0.6, the addition of 0.4 mM IPTG was followed by cells incubation for 4 h at 27°C. Cells were harvested by centrifugation (4400 rpm, 40 min, 4°C), and 1 L of expression was resuspended in 15 mL of buffer (20 mM Tris-HCl, pH 7.5, 100 mM KCl) and stored at −20°C. For purification, the frozen cells were resuspended in 50 mL of lysis buffer (20 mM Tris-HCl, pH 7.5, 100 mM KCl, 2 mg/mL lysozyme, 50 μL/mL benzonase, and 1 mM PMSF). Lysis was performed using an ultrasound probe (amplitude 25; pulse-on 25 s; pulse-off 30 s) for 10 min. The lysate was centrifuged at 11 000 × *g* for 40 min at 4°C, and the soluble fraction was purified in three steps: (1) Chromatography using an MBPTrap column (1 mL); (2) Proteolytic cleavage with TEV protease; (3) Purification on a HisTrap column (5 mL). The final protein was concentrated and stored in freezing buffer (20 mM Tris-HCl pH 7.5, 100 mM KCl, 10% glycerol) [11].

4.9 | Enzyme Inhibition Assay

To evaluate the inhibition of the extracts against the *Pf*PyrKII, a coupled assay using PyrKII and luciferase enzymes was performed [63]. The reaction mixture (Mix I) contained 100 mM MOPS buffer (pH 7.4), 1.0 mM β-mercaptoethanol, 1.5 mM $MgCl_2$, 1.0 mM ADP, and 50 nM PyrKII, in a total volume of 50 μL. Test samples (0.5 μL of 5 mg/mL stock solution) were added to 46.5 μL of Mix I and incubated for 20 min at 37°C.

After, 3 μL of phosphoenolpyruvate (PEP; final concentration 40 μM) was added, followed by another 20 min incubation at 37°C. Subsequently, 50 μL of the Kinase Glo Plus reagent (Promega) was added, and luminescence was measured at 550 nm after 5 min of incubation. A positive control (Mix I and PEP) and a negative control (Mix I only) were used.

4.10 | Molecular Modeling

The three-dimensional structure of *Pf*PyrKII was generated using AlphaFold2 [64] based on its primary amino acid sequence and the crystallographic structures of *P. falciparum* PyrKI (*Pf*PyrKI; PDB: 6KHS) as template. To guide model interpretation and placement of cofactor, we aligned the resulting structure with the crystallographic structures of *Pf*PyrKI (PDB: 6KHS), co-crystallized with oxalate and ATP, and the rabbit muscle pyruvate kinase (PDB: 1A49). From this structural alignment, Mg^{2+} ions and coordinating water molecules were manually inserted into the *Pf*PyrKII model. Protonation states of the amino acid residues were assigned using PDB2PQR [65] at pH 7.5, matching the assay conditions.

The SMILES string of procyanidin A1 was converted into a 3D structure (mol2 format) using Open Babel. Its ionization state at physiological pH was verified with FixpKa [66] (OpenEye). Molecular docking was performed using GOLD [67], considering Mg^{2+} and the coordinating waters as part of the binding site. GOLD was configured to evaluate whether the structural water should be retained or displaced during docking. Binding pockets in the *Pf*PyrKII model were identified and analyzed using KVFinder Web [59, 60], which allowed calculation of cavity volume and spatial distribution based on the protein's 3D conformation. The binding site was defined as a 20 Å sphere centered at $x = 0.000$, $y = 13$, and $z = 5$, corresponding to the ATP binding site in PDB 6KHS. Docking poses were visually evaluated, with special attention to hydrogen bonding and the coordination geometry around Mg^{2+}.

Author Contributions

Thais Bertolino Vieira Dantas: (master student) analyzed all data, carried out compound isolation, conducted the GC–MS experiment and drafted the manuscript. **Romário Pereira da Costa**: optimized the preparative HPLC conditions for the isolation of procyanidin A1. **Quezia Bezerra Cass**: contributed to the optimization of the LC-HRMS method for extract analysis and provided critical revisions of the manuscript. **Guilherme Eduardo de Souza**: conducted experiments against *P. falciparum* and pyruvate kinase II. **Igor M. R. Moura**: conducted experiments against *P. falciparum* and pyruvate kinase II. **Hélder Nagai Consolaro**: assisted in plant sample collection and botanical identification. **Richele Priscila Severino**: contributed with critical reading of the manuscript. **Luis Felipe de Oliveira**: carried out the molecular docking studies of procyanidin A1 with *Pf*PyrKII. **Vinicius Bonatto**: carried out the molecular docking studies of procyanidin A1 with *Pf*PyrKII. **Rafael V. C. Guido**: supervised the research work, contributed with data interpretation (biological results) and in writing and reviewing the manuscript. **Lorena Ramos Freitas de Sousa**: supervised the research work, contributed with data interpretation (NMR and MS results) and in writing and reviewing the manuscript. All the authors read and approved the final version of the manuscript.

Acknowledgments

This research received financial support from the FAPEG (Goiás State Research Support Foundation) Proc. 202110267000075, FAPESP (The São Paulo Research Foundation, grants #20/12904-5; #24/04805-8; #13/07600-3; #23/15815-1; #23/09209-1, #14/50244-6; #21/03977-1), and the National Council for Scientific and Technological Development (CNPq, Conselho Nacional de Pesquisa e Desenvolvimento), Brazil (302464/2022-0). The authors wish to thank the Multi-User Laboratory at the Federal University of Uberlândia (NMR experiments at 400 MHz spectrometer), to Dr. L. R. G. da Silva for LC-HRMS analysis, Dr. A. G. Ferreira for NMR acquisition at 600 MHz spectrometer and Dr. M. F. das G. F. da Silva for providing access to HPLC equipment for compound purification.

The Article Processing Charge for the publication of this research was funded by the Coordenação de Aperfeiçoamento de Pessoal de Nível Superior - Brasil (CAPES) (ROR identifier: 00x0ma614).

Conflicts of Interest

The authors declare no conflict of interest.

Data Availability Statement

The data that support the findings of this study are available from the corresponding author upon reasonable request.

References

1. World Health Organization, "*World Malaria Report 2024: Addressing Inequity in the Global Malaria Response*," accessed 16 January 2025,

https://www.who.int/teams/global-malaria-programme/reports/world-malaria-report-2024.

2. Bvsms, "*Guia de tratamento da malária no Brasil*," accessed 05 June 2024, https://bvsms.saude.gov.br/bvs/publicacoes/guia_tratamento_malaria_brasil.pdf.

3. W. Amelo and E. Makonnen, "Efforts Made to Eliminate Drug-resistant Malaria and Its Challenges," *BioMed Research International* 2021 (2021): 5539544, https://doi.org/10.1155/2021/5539544.

4. X. Z. Su, K. D. Lane, L. Xia, J. M. Sá, and T. E. Wellems, "*Plasmodium* Genomics and Genetics: New Insights Into Malaria Pathogenesis, Drug Resistance, Epidemiology, and Evolution," *Clinical Microbiology Reviews* 32 (2019): e00019–19, https://doi.org/10.1128/CMR.00019-19.

5. A. Uwimana, E. Legrand, B. H. Stokes, et al., "Emergence and Clonal Expansion of *In Vitro* Artemisinin-Resistant *Plasmodium falciparum kelch13* R561H Mutant Parasites in Rwanda," *Nature Medicine* 26 (2020): 1602–1608, https://doi.org/10.1038/s41591-020-1005-2.

6. A. C. Aguiar, L. R. F. de Sousa, C. R. S. Garcia, G. Oliva, and R. V. C. Guido, "New Molecular Targets and Strategies for Antimalarial Discovery," *Current Medicinal Chemistry* 25 (2018): 4380–4402, https://doi.org/10.2174/0929867324666170830103003.

7. C. D. Goodman and G. I. Mcfadden, "Targeting Apicoplasts in Malaria Parasites," *Expert Opinion on Therapeutic Targets* 17 (2012): 167–177, https://doi.org/10.1517/14728222.2013.739158.

8. T. Maeda, T. Saito, O. S. Harb, et al., "Pyruvate Kinase Type II Isozyme in *Plasmodium falciparum* Localizes to the Apicoplast," *Parasitology International* 58 (2009): 101–105, https://doi.org/10.1016/j.parint.2008.10.005.

9. A. Mukherjee and G. C. Sadhukhan, "Anti-Malarial Drug Design by Targeting Apicoplasts: New Perspectives," *Journal of Pharmacopuncture* 19 (2016): 7–15, https://doi.org/10.3831/KPI.2016.19.001.

10. W. Zhong, K. Li, Q. Cai, et al., "Pyruvate Kinase From *Plasmodium falciparum*: Structural and Kinetic Insights Into the Allosteric Mechanism," *Biochemical and Biophysical Research Communications* 532 (2020): 370–376, https://doi.org/10.1016/j.bbrc.2020.08.048.

11. R. P. Swift, K. Rajaram, C. Keutcha, et al., "The NTP Generating Activity of Pyruvate Kinase II Is Critical for Apicoplast Maintenance in *Plasmodium falciparum*," *eLife* 9 (2020): e50807, https://doi.org/10.7554/eLife.50807.

12. P. K. Boniface and E. I. Ferreira, "Flavonoids as Efficient Scaffolds: Recent Trends for Malaria, Leishmaniasis, Chagas Disease, and Dengue," *Phytotherapy Research* 33 (2019): 2473–2517, https://doi.org/10.1002/ptr.6383.

13. E. Fernández-Álvaro, W. D. Hong, G. L. Nixon, P. M. O'Neill, and F. Calderón, "Antimalarial Chemotherapy: Natural Product Inspired Development of Preclinical and Clinical Candidates With Diverse Mechanisms of Action," *Journal of Medicinal Chemistry* 59 (2016): 5587–5603, https://doi.org/10.1021/acs.jmedchem.5b01485.

14. D. J. Newman and G. M. Cragg, "Natural Products as Sources of New Drugs Over the 30 Years From 1981 to 2010," *Journal of Natural Products* 75 (2012): 311–335, https://doi.org/10.1021/np200906s.

15. Y. Tu, "The Discovery of Artemisinin (Qinghaosu) and Gifts From Chinese Medicine," *Nature Medicine* 17 (2011): 1217–1220, https://doi.org/10.1038/nm.2471.

16. N. Beldjoudi, L. Mambu, M. Labaïed, et al., "Flavonoids From *Dalbergia louvelii* and Their Antiplasmodial Activity," *Journal of Natural Products* 66 (2003): 1447–1450, https://doi.org/10.1021/np030008x.

17. A. Salatino, M. J. P. Ferreira, R. G. Udulutsch, C. E. Palacios, and M. L. F. Salatino, "Fingerprint of *Cerrado* Species Based on Cork Lipophilic Constituents," *Biochemical Systematics and Ecology* 88 (2020): 103989, https://doi.org/10.1016/j.bse.2019.103989.

18. E. L. Silva, L. L. P. F. Moreira, W. C. Cardoso, et al., "Inhibitory Activity and Docking Studies of Cathepsin V for Isoflavanoids From *Dalbergia miscolobium* Benth," *Revista Virtual de Química* 13 (2021): 136–145, https://doi.org/10.21577/1984-6835.20200135.

19. A. N. Panche, A. D. Diwan, and S. R. Chandra, "Flavonoids: An Overview," *Journal of Nutritional Science* 5 (2016): e457, https://doi.org/10.1017/jns.2016.41.

20. M. C. Jonville, H. Kodja, L. Humeau, et al., "Screening of Medicinal Plants From Reunion Island for Antimalarial and Cytotoxic Activity," *Journal of Ethnopharmacology* 120 (2008): 382–386, https://doi.org/10.1016/j.jep.2008.09.005.

21. A. Singh, H. M. Mukhtar, H. Kaur, and L. Kaur, "Investigation of Antiplasmodial Efficacy of Lupeol and Ursolic Acid Isolated From *Ficus benjamina* Leaves Extract," *Natural Product Research* 34 (2018): 2514–2517, https://doi.org/10.1080/14786419.2018.1540476.

22. M. D. Rush, E. A. Rue, A. M. Wong, P. Kowalski, J. A. Glinski, and R. B. V. Breemen, "Rapid Determination of Procyanidins Using MALDI-ToF/ToF Mass Spectrometry," *Journal of Agricultural and Food Chemistry* 66 (2018): 11355–11361, https://doi.org/10.1021/acs.jafc.8b04258.

23. A. Engemann, F. Hübner, S. Rzeppa, and H. U. Humpf, "Intestinal Metabolism of Two A-Type Procyanidins Using the Pig Cecum Model: Detailed Structure Elucidation of Unknown Catabolites With Fourier Transform Mass Spectrometry (FTMS)," *Journal of Agricultural and Food Chemistry* 60 (2012): 749–757, https://doi.org/10.1021/jf203927g.

24. J. G. Kang, L. A. Hick, and W. E. Price, "A Fragmentation Study of Isoflavones in Negative Electrospray Ionization by MSn Ion Trap Mass Spectrometry and Triple Quadrupole Mass Spectrometry," *Rapid Communications in Mass Spectrometry* 21 (2007): 857–868, https://doi.org/10.1002/rcm.2897.

25. D. Tian, Y. Yang, M. Yu, et al., "Anti-Inflammatory Chemical Constituents of *Flos Chrysanthemi Indici* Determined by UPLC-MS/MS Integrated With Network Pharmacology," *Food & Function* 11 (2020): 6340–6351, https://doi.org/10.1039/D0FO01000F.

26. C. Barnaba, E. Dellacasa, G. Nicolini, T. Nardin, M. Malacarne, and R. Larcher, "Free and Glycosylated Simple Phenol Profiling in Apulian Italian Wines," *Food Chemistry* 206 (2016): 260–266, https://doi.org/10.1016/j.foodchem.2016.03.040.

27. S. Fetni, N. Bertella, and A. Ouahab, "LC-DAD/ESI-MS/MS Characterization of Phenolic Constituents in *Rosa canina* L. and Its Protective Effect in Cells," *Biomedical Chromatography* 34 (2020): e4961, https://doi.org/10.1002/bmc.4961.

28. K. S. R. Raju, N. Kadian, I. Taneja, and M. Wahajuddin, "Phytochemical Analysis of Isoflavonoids Using Liquid Chromatography Coupled With Tandem Mass Spectrometry," *Phytochemistry Reviews* 14 (2015): 469–498, https://doi.org/10.1007/s11101-015-9400-x.

29. C. M. Wang, Y. M. Hsu, Y. L. Jhan, et al., "Structure Elucidation of Procyanidins Isolated From *Rhododendron formosanum* and Their Anti-Oxidative and Anti-Bacterial Activities," *Molecules* 20 (2015): 12787–12803, https://doi.org/10.3390/molecules200712787.

30. Z. J. Suárez-Montenegro, D. Ballesteros-Vivas, R. Gallego, et al., "Neuroprotective Potential of Tamarillo (*Cyphomandra betacea*) Epicarp Extracts Obtained by Sustainable Extraction Process," *Frontiers in Nutrition* 8 (2021): 769617, https://doi.org/10.3389/fnut.2021.769617.

31. B. Attioua, L. Lagnika, D. Yeo, et al., "*In Vitro* Antiplasmodial and Antileishmanial Activities of Flavonoids From *Anogeissus leiocarpus* (Combretaceae)," *International Journal of Pharmaceutical Sciences Review and Research* 11 (2011): 1–6.

32. P. H. B. de Moura, A. A. de Sousa, A. Porzel, L. A. Wessjohann, I. C. R. Leal, and R. C. C. Martins, "Characterization of Antibacterial Proanthocyanidins of *Dalbergia monetaria*, an Amazonian Medicinal Plant, by UHPLC-HRMS/MS," *Planta Medica* 86 (2020): 858–866, https://doi.org/10.1055/a-1170-8016.

33. D. S. Nunes, A. Haag, and H. J. Bestmann, "Two Proanthocyanidins From the Bark of *Dalbergia monetari*," *Phytochemistry* 28 (1989): 2183–2186, https://doi.org/10.1016/S0031-9422(00)97940-8.

34. J. P. Abdou, J. Momeni, A. Adhikari, et al., "New Coumestan and Coumaronochromone Derivatives From *Dalbergia boehmii* Taub. (Fabaceae)," *Phytochemistry Letters* 21 (2017): 109–113, https://doi.org/10.1016/j.phytol.2017.06.014.

35. P. H. B. de Moura, W. Brandt, A. Porzel, R. C. C. Martins, I. C. R. Leal, and L. A. Wessjohann, "Structural Elucidation of an Atropisomeric Entcassiflavan-(4β→8)-Epicatechin Isolated From *Dalbergia monetaria* L.F. Based on NMR and ECD Calculations in Comparison to Experimental Data," *Molecules* 27 (2022): 2512, https://doi.org/10.3390/molecules27082512.

36. P. Borai and R. Dayal, "A Flavone Glycoside From *Dalbergia stipulacea* Leaves," *Phytochemistry* 33 (1993): 731–732, https://doi.org/10.1016/0031-9422(93)85488-D.

37. E. L. Silva, L. L. P. F. Moreira, W. C. Cardoso, et al., "Inhibitory Activity and Docking Studies of Cathepsin V for Isoflavanoids From *Dalbergia miscolobium* Benth," *Revista Virtual de Química* 13 (2021): 136–145, https://doi.org/10.21577/1984-6835.20200135.

38. S. N. The, "A Review on the Medicinal Plant *Dalbergia odorifera* Species: Phytochemistry and Biological Activity," *Evidence-Based Complementary and Alternative Medicine* 2017 (2017): 7142370, https://doi.org/10.1155/2017/7142370.

39. Á. Szatmári, A. M. Móricz, I. Schwarczinger, et al., "A Pattern-Triggered Immunity-Related Phenolic, Acetosyringone, Boosts Rapid Inhibition of a Diverse Set of Plant Pathogenic Bacteria," *BMC Plant Biology* 21 (2021): 153, https://doi.org/10.1186/s12870-021-02928-4.

40. A. A. Carvalho, L. R. Dos Santos, J. S. de Freitas, and M. H. Chaves, "Isoflavonoides Da Tribo Dalbergieae: Uma Contribuição Quimiossistemática para a Subfamília papilionoideae," *Quimica Nova* 43 (2020): 1294–1311, https://doi.org/10.21577/0100-4042.20170588.

41. C. Kraft, K. Jenett-Siems, K. Siems, M. P. Gupta, U. Bienzle, and E. Eich, "Antiplasmodial Activity of Isoflavones From *Andira inermis*," *Journal of Ethnopharmacology* 73 (2000): 131–135, https://doi.org/10.1016/S0378-8741(00)00285-3.

42. G. Duker-Eshun, J. W. Jaroszewski, W. A. Asomaning, F. Oppong-Boachie, and S. B. Christensen, "Antiplasmodial Constituents of *Cajanus cajan*," *Phytotherapy Research* 18 (2004): 128–130, https://doi.org/10.1002/ptr.1375.

43. L. T. Lôbo, K. C. F. Castro, M. S. P. Arruda, et al., "Potencial Alelopático de catequinas de *Tachigali Myrmecophyla* (leguminosae)," *Quimica Nova* 31 (2008): 493–497, https://doi.org/10.1590/S0100-40422008000300005.

44. D. Torres-Mendoza, J. González, E. Ortega-Barría, et al., "Weakly Antimalarial Flavonol Arabinofuranosides From *Calycolpus warszewiczianus*," *Journal of Natural Products* 69 (2006): 826–828, https://doi.org/10.1021/np050484i.

45. A. R. Sannella, L. Messori, A. Casini, et al., "Antimalarial Properties of Green Tea," *Biochemical and Biophysical Research Communications* 353 (2007): 177–181, https://doi.org/10.1016/j.bbrc.2006.12.005.

46. S. Prachayasittikul, P. Saraban, R. Cherdtrakulkiat, S. Ruchirawat, and V. Prachayasittikul, "New Bioactive Triterpenoids and Antimalarial Activity of *Diospyros rubra* Lec," *EXCLI Journal* 9 (2010): 1–10.

47. C. V. S. Prakash and I. Prakash, "Isolation and Structural Characterization of Lupane Triterpenes From *Polypodium vulgare*," *Research Journal of Pharmaceutical Sciences* 1 (2012): 23–27, https://doi.org/10.7897/2230-8407.09347.

48. W. Buakaew, S. R. Pankla, C. Noysang, et al., "Phytochemical Constituents of *Citrus hystrix* DC. Leaves Attenuate Inflammation via NF-kB Signaling and NLRP3 Inflammasome Activity in Macrophages," *Biomolecules* 11 (2021): 105–117, https://doi.org/10.3390/biom11010105.

49. A. Suksamrarn, T. Tanachatchairatana, and S. Kanokmedhakul, "Antiplasmodial Triterpenes From Twigs of *Gardenia saxatilis*," *Journal of Ethnopharmacology* 88 (2003): 275–277, https://doi.org/10.1016/S0378-8741(03)00261-7.

50. R. P. Adams, *Identification of Essencial Oils Components by Gas Chromatography/Mass Spectrometry* (Allured Publishing Corporation: Illinois, 2017).

51. J. A. Pino, J. Mesa, Y. Muñoz, M. P. Martí, and R. Marbot, "Volatile Components From Mango (*Mangifera indica* L.) Cultivars," *Journal of Agricultural and Food Chemistry* 53 (2005): 2213–2223, https://doi.org/10.1021/jf0402633.

52. H. J. D. Lalel, Z. Singh, and S. C. Tan, "Glycosidically-bound Aroma Volatile Compounds in the Skin and Pulp of 'Kensington Pride' Mango Fruit at Different Stages of Maturity," *Postharvest Biology and Technology* 29 (2003): 205–218, https://doi.org/10.1016/S0925-5214(02)00250-8.

53. A. P. Oluyori, C. Nwonuma, T. Akpo, et al., "In Vivo Antiplasmodial Potential of the Leaf, Mesocarp, and Epicarp of the *Raphia hookeri* Plant in Mice Infected With *Plasmodium berghei* NK65," *Evid-Based Complementary and Alternative Medicine* 2022 (2022): 4129045, https://doi.org/10.1155/2022/4129045.

54. T. Tyagi and M. Argawal, "Phytochemical Screening and GC-MS Analysis of Bioactive Constituents in the Ethanolic Extract of *Pistia stratiotes* L. and *Eichhornia crassipes* (Mart.) Solms," *Journal of Pharmacognosy and Phytochemistry* 6 (2017): 195–206.

55. J. E. Okokon, B. S. Antia, D. Mohanakrishnan, and D. Sahal, "Antimalarial and Antiplasmodial Activity of Husk Extract and Fractions of *Zea mays*," *Pharmaceutical Biology* 55 (2017): 1394–1400, https://doi.org/10.1080/13880209.2017.1302966.

56. J. P. Daily, "Antimalarial Drug Therapy: The Role of Parasite Biology and Drug Resistance," *Journal of Clinical Pharmacology* 46 (2006): 1487–1497, https://doi.org/10.1177/0091270006294276.

57. M. Madamet, S. Briolant, R. Amalvict, et al., "The *Plasmodium falciparum* Chloroquine Resistance Transporter Is Associated With the Ex Vivo *P. falciparum* African Parasite Response to Pyronaridine," *Parasites & Vectors* 9 (2016): 77, https://doi.org/10.1186/s13071-016-1358-z.

58. K. P. Godinez-Macias, D. Chen, J. L. Wallis, et al., "Revisiting the *Plasmodium falciparum* Druggable Genome Using Predicted Structures and Data Mining," *npj Drug Discovery* 2 (2025): 3, https://doi.org/10.1038/s44386-025-00006-5.

59. J. V. S. Guerra, H. V. Ribeiro-Filho, J. G. C. Pereira, and P. S. Lopes-de-oliveira, "KVFinder-Web: A Web-based Application for Detecting and Characterizing Biomolecular Cavities," *Nucleic Acids Research* 51 (2023): W289–W297, https://doi.org/10.1093/nar/gkad324.

60. J. V. da S. Guerra, H. V. Ribeiro Filho, et al., "ParKVFinder: A Thread-Level Parallel Approach in Biomolecular Cavity Detection," *SoftwareX* 12 (2020): 100606, https://doi.org/10.1016/j.softx.2020.100606.

61. M. Smilkstein, N. Sriwilaijaroen, J. X. Kelly, P. Wilairat, and M. Riscoe, "Simple and Inexpensive Fluorescence-Based Technique for High-Throughput Antimalarial Drug Screening," *Antimicrobial Agents and Chemotherapy* 48 (2004): 1803–1806, https://doi.org/10.1128/AAC.48.5.1803-1806.2004.

62. T. Mosmann, "Rapid Colorimetric Assay for Cellular Growth and Survival: Application to Proliferation and Cytotoxicity Assays," *Journal of Immunological Methods* 65 (1983): 55–63, https://doi.org/10.1016/0022-1759(83)90303-4.

63. S. Mohammadi, M. Nikkhah, M. Nazari, and S. Hosseinkhani, "Design of a Coupled Bioluminescent Assay for a Recombinant Pyruvate Kinase From a Thermophilic *Geobacillus*," *Photochemistry and Photobiology* 87 (2011): 1338–1345, https://doi.org/10.1111/j.1751-1097.2011.00973.x.

64. M. Mirdita, K. Schütze, Y. Moriwaki, L. Heo, S. Ovchinnikov, and M. Steinegger, "ColabFold: Making Protein Folding Accessible to All," *Nature Methods* 19 (2022): 679–682, https://doi.org/10.1038/s41592-022-01488-1.

65. E. Jurrus, D. Engel, K. Star, et al., "Improvements to the APBS Biomolecular Solvation Software Suite," *Protein Science* 27 (2018): 112–128, https://doi.org/10.1002/pro.3280.

66. QUACPAC 2.2.5.1. OpenEye. "*Cadence Molecular Sciences: Santa Fe*," accessed June 5, 2024, http://www.eyesopen.com.

67. G. Jones, P. Willett, R. C. Glen, A. R. Leach, and R. Taylor, "Development and Validation of a Genetic Algorithm for Flexible Docking," *Journal of Molecular Biology* 267 (1997): 727–748, https://doi.org/10.1006/jmbi.1996.0897.

Supporting Information

Additional supporting information can be found online in the Supporting Information section.